Primary Frequency Control of DFIG-WTs Using Bang-bang Phase Angle Controller

ISSN 1751-8644
doi: 0000000000

Y. Liu[1], *L. Jiang*[2], *J. S. Smith*[2], *Q. H. Wu*[1,2*]

[1] *School of Electric Power Engineering, South China University of Technology, Guangzhou, 510640, China.*
[2] *Department of Electrical Engineering and Electronics, The University of Liverpool, Liverpool, L69 3GJ, U.K.*
** E-mail: wuqh@scut.edu.cn*

Abstract: A bang-bang phase angle controller (BPAC) was proposed in this paper for the primary frequency control of doubly-fed induction generator-based wind turbines (DFIG-WT). Dynamics of the internal voltage of a synchronous generator (SG) and that of a DFIG-WT were investigated in frequency deviation events. A bang-bang phase angle controller (BPAC) was designed to regulate the phase angle obtained with a phase-locked loop (PLL) directly, which enables the rapid active power control of the DFIG-WT. The BPAC signal is fed into the active power regulation loop of the pitch angle controller, which is expected to help rotor speed recovery and prevent secondary frequency drop. Small-signal analysis was carried out for the closed-loop system, composed of the DFIG-WT and the external synchronous generator-based power system, to verify the stability of the overall system. Simulation studies were undertaken on a wind power penetrated multi-machine power system, through which the primary frequency control performance of the BPAC was verified.

1 Introduction

Due to the power electronics interfaces, the dynamics of wind power generators is decoupled from that of the external power grid [1-3]. As such, wind power generators provide little frequency support to the external power grid. The frequency stability of power systems having large-scale wind power penetration is an increasingly prominent problem of concern as the rapid development of wind power generation [4-6]. Many investigations were undertaken to solve this problem, which can be classified into the following two groups: the methods based on conventional PLL synchronization techniques and the methods based on direct energy balancing synchronization techniques.

With respect to the methods based on the conventional PLL synchronization techniques, the concept of virtual synchronous generator was proposed in [7]. Within this study, short-term energy storage was connected to the renewable energy generators such that they can perform like synchronous generators and provide virtual inertia to the external grid. Similar results were presented in [8,9], in which a virtual inertia control method was realized by connecting a rotating mass to the DFIG-WT shaft or a super-capacitor to the DC-link of the converters of a DFIG-WT. However, these techniques would introduce additional cost to the wind power plants. In [10], the inertia emulation of wind turbines was achieved by adding the frequency deviation and its first-order derivative into the torque control loop of the wind power generator. Apparently, this method requires that the measurement noise of system frequency is low, otherwise, the noise could introduce additional disturbances to the speed control loop of wind power generators. The frequency droop controller was introduced in the active power control loop of wind power generators to mimic the governor of SGs [11]. This enables the wind power generator to respond to any frequency excursions of the external grids. Nevertheless, the correct operation of the droop controller relies on the dynamics of the active power control loop of the wind power generator. Without elaborate coordination, it could further deteriorate the frequency dynamics of the external grid.

In terms of the techniques that achieve synchronization with the external grid through direct energy balancing, the concept of synchronverters has drawn a lot of attention. In [12], an inverter was operated as a SG by implementing the model of a SG in its control loop. In this way, the inverter synchronizes with external grids through direct energy balancing, i.e. the frequency- and voltage-drooping mechanism of the SG. The synchronverter has some beneficial characteristics of the SG, however, it also has the drawbacks of the SG, such as going unstable due to under-excitation and low frequency oscillations [13]. A virtual synchronous control method was proposed for the control of DFIG-WTs in [14]. In this work, a SG model was embedded within the speed control loop of the DFIG-WT to achieve automatic synchronization with the power grid. However, it has the drawbacks of SGs as well and the control of the grid-side converter has not been discussed. Moreover, the simulation studies of the previous literatures [7,8,10-14] neglected the switching dynamics of the IGBTs of the converters in system models. Thus the proposed controllers cannot be evaluated in a practical manner.

Concerning that the PLL-based vector control system has already been widely applied in wind power generators, using a completely novel control scheme, such as the synchronization techniques based on direct energy balancing, will complicate the control system and introduce additional cost to the wind power plants [15], this paper introduces a BPAC to regulate the relative phase position of the internal voltage of the DFIG-WT by adding a bang-bang control signal to the output of the PLL. The active power output of the DFIG-WT is largely determined by relative spacial position of its internal voltage vector and its terminal bus voltage vector [16]. Therefore, the active power output of the DFIG-WT can be controlled by the BPAC accordingly. The kinetic energy stored in the rotor and wind turbine is released or restored to provide primary frequency support to the external power grid. To get rid of the secondary frequency drop or overshot during the process of rotor speed recovery, the output of the BPAC is also fed to the pitch angle controller. The remaining configuration of the vector control system remains unchanged.

The BPAC is designed based on the bang-bang funnel controller [17], which involves logic calculation only [18]. Compared with the virtual synchronous generator techniques [7,8], the BPAC does not need any additional hardware and works on the basis of the traditional vector control system. In contrast to the inertia emulation scheme presented in [10], the BPAC is triggered by the magnitude of frequency deviation and thus has stronger robustness to measurement noise. The BPAC directly regulates the phase position of the internal voltage of the DFIG-WT and the active power reference in pitch angle controller, which are not sensitive to the dynamics of the controller of the rotor-side converter. Hence, the primary frequency control performance of the BPAC is less influenced by the active power control loop of the DFIG-WT compared with the droop control method investigated in [11].

Overall, this paper is organized as follows. Section 2 presents the different frequency response mechanisms of the SG and the DFIG-WT. The dynamics of the internal voltage of a SG and a DFIG-WT are analyzed in frequency excursion events, respectively. Section 3 is dedicated to BPAC design. Then the small signal analysis is presented in Section 4 to verify the closed-loop stability of the overall system. Simulation studies were performed in Section 5 on a wind power penetrated multi-machine power system. Discussions and conclusions are draw in Section 6 and Section 7, respectively.

2 The Dynamics of the Internal Voltage of Synchronous Generators and DFIG-WTs in Frequency Excursion Events

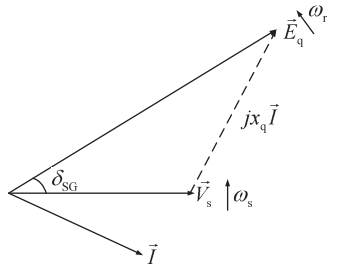

(a) Schematic of the motion of the voltage vectors of a SG.

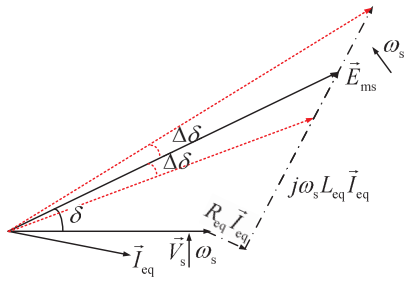

(b) Schematic of the motion of the voltage vectors of a DFIG-WT.

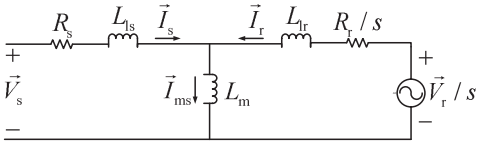

(c) Equivalent circuit of a DFIG-WT.

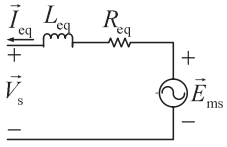

(d) Equivalent circuit of the one presented in (c).

Fig. 1: Schematic of the motion of the voltage vectors of a SG and those of a DFIG-WT, and the equivalent circuits of a DFIG-WT.

2.1 Dynamics of the internal voltage vector of a SG in frequency excursion events

With the change of rotor angle, i.e., $\delta_{\rm SG}$ in Fig. 1 (a), the kinetic energy stored in the rotor of the SG is released or restored to reduce the external frequency error. According to Fig. 1 (a), the terminal bus voltage vector $\overrightarrow{V}_{\rm s}$ rotates with speed $\omega_{\rm s}$, which is the frequency of the external power grid. The internal voltage vector $\overrightarrow{E}_{\rm q}$ rotates with speed $\omega_{\rm r}$, which equals p (the number of pole pairs) -times of the mechanical rotating speed $\Omega_{\rm r}$ of the rotor of the SG. It should be noted that $\omega_{\rm s}$ is determined by the rotor speed of all the SGs in the power grid. Thus $\omega_{\rm s}$ is not necessarily equal to $\omega_{\rm r}$ unless there is only one SG in the power grid.

In the case where the frequency of the external grid ω_s decreases, the electrical rotor angle $\delta_{\rm SG} = \int(\omega_{\rm r} - \omega_{\rm s})dt$ will increase. Regarding the case of a SG, the active power is $P_{\rm eSG} = \frac{E_{\rm q}V_{\rm s}}{x_{\rm q}}\sin(\delta_{\rm SG})$, the active power output of the SG will increase to support the frequency decrease of the external grid. According to the motion equation of the rotor, i.e. $\dot{\omega}_{\rm r} = \frac{1}{2H}(P_{\rm mSG} - P_{\rm eSG})$, the rotor speed $\omega_{\rm r}$ will then decrease since the change of mechanical input $P_{\rm mSG}$ of a SG is much slower than the variation of electromechanical power output. Therefore, the active power output of the SG is composed of two parts. The first part is the mechanical power input $P_{\rm mSG}$, and the second part is the released kinetic energy of the rotor. The dynamics of a SG in the case of a frequency increase follows analogously. Moreover, the above behavior of the SG is referred to as inertial response.

From the view of the external power grid, the inertial response of the SG results from the motion of its rotor angle $\delta_{\rm SG}$. For the case of a DFIG-WT, its rotor side dynamics is decoupled from the external power grid by the power converters and the vector control system. Thus the internal dynamics of a DFIG-WT should be studied before the BPAC design.

2.2 The Dynamics of the Internal Voltage of a DFIG-WT

The steady-state model of a DFIG-WT can be written as [1],

$$\begin{cases} \overrightarrow{V}_{\rm s} = R_{\rm s}\overrightarrow{I}_{\rm s} + j\omega_{\rm s}L_{\rm ls}\overrightarrow{I}_{\rm s} + j\omega_{\rm s}L_{\rm m}(\overrightarrow{I}_{\rm s} + \overrightarrow{I}_{\rm r}) \\ \frac{\overrightarrow{V}_{\rm r}}{s} = \frac{R_{\rm r}}{s}\overrightarrow{I}_{\rm r} + j\omega_{\rm s}L_{\rm lr}\overrightarrow{I}_{\rm r} + j\omega_{\rm s}L_{\rm m}(\overrightarrow{I}_{\rm s} + \overrightarrow{I}_{\rm r}) \end{cases} \quad (1)$$

where $\overrightarrow{V}_{\rm s}$ is the terminal bus voltage of the DFIG-WT, $R_{\rm s}$ is the resistance of the stator windings, $\overrightarrow{I}_{\rm s}$ denotes the current of the stator windings, $\omega_{\rm s}$ denotes the frequency of $\overrightarrow{V}_{\rm s}$, which is also the frequency of the external power grid, $L_{\rm ls}$ represents the leakage inductance of the stator windings, $L_{\rm m}$ denotes the mutual inductance, $\overrightarrow{I}_{\rm r}$ is the current of the rotor windings, s represents the slip speed and is defined as $s = (\omega_{\rm s} - \omega_{\rm r})/\omega_{\rm s}$, $\overrightarrow{V}_{\rm r}$ denotes the excitation voltage of the rotor windings, which is also the output voltage of the rotor-side converter, $R_{\rm r}$ is the resistance of the rotor windings, $L_{\rm lr}$ denotes the leakage inductance of the rotor windings [1]. Then the DFIG-WT circuit is represented as depicted in Fig. 1 (c), in which $\overrightarrow{I}_{\rm ms}$ represents the magnetizing current. Then this circuit is rearranged to the one presented in Fig. 1 (d), where $R_{\rm eq} = R_{\rm s} + \frac{\omega_{\rm s}^2 L_{\rm m}^2 R_{\rm r}/s}{(R_{\rm r}/s)^2 + (\omega_{\rm s}L_{\rm r})^2}$, $L_{\rm eq} = L_{\rm ls} + \frac{L_{\rm m}[\omega_{\rm s}^2 L_{\rm lr}L_{\rm r} + (R_{\rm r}/s)^2]}{(R_{\rm r}/s)^2 + (\omega_{\rm s}L_{\rm m})^2}$, $L_{\rm r} = L_{\rm lr} + L_{\rm m}$ is the rotor inductance, and $\overrightarrow{E}_{\rm ms} = \frac{s\omega_{\rm s}^2 L_{\rm m}(L_{\rm m}+L_{\rm lr}) + j\omega_{\rm s}L_{\rm m}R_{\rm r}}{R_{\rm r}^2 + [s\omega_{\rm s}(L_{\rm m}+L_{\rm lr})]^2}\overrightarrow{V}_{\rm r}$ is the internal voltage of the DFIG-WT. Fig. 1 (b) presents the voltage vectors of the DFIG-WT.

As presented by Fig. 1 (b), the terminal bus voltage vector $\overrightarrow{V}_{\rm s}$ rotates with speed $\omega_{\rm s}$, which is the frequency of the external power grid. The internal voltage $\overrightarrow{E}_{\rm ms}$ is generated by the stator windings through cutting the rotating magnetic field generated by the rotor. The difference between the rotating speed of the rotor and the grid frequency is compensated by the frequency of the rotor excitation voltage generated by the rotor-side converter. In this way, the rotating speed of the rotor magnetic field is composed of two parts. The first part is the rotating speed of the rotor, and the second part is the rotating speed of the rotor excitation voltage. By adding these two parts, the obtained rotating speed of the rotor magnetic field equals the grid frequency $\omega_{\rm s}$. Hence, the rotating speed of the internal voltage $\overrightarrow{E}_{\rm ms}$ is $\omega_{\rm s}$. Therefore, it has been shown that $\overrightarrow{E}_{\rm ms}$ and $\overrightarrow{V}_{\rm s}$ rotate at the same speed. Thus the angle δ is constant. Therefore, the frequency change of the external grids can only influence the voltage drop on $L_{\rm eq}$, i.e. $j\omega_{\rm s}L_{\rm eq}$. Due to the limited value of $\overrightarrow{I}_{\rm s}$ and $L_{\rm eq}$, the frequency response of the DFIG-WT through the change of $j\omega_{\rm s}L_{\rm eq}\overrightarrow{I}_{\rm s}$ is small.

, pp. 1–9

In order to improve the frequency response capability of the DFIG-WT, it is desirable that the internal voltage $\vec{E}_{\rm ms}$ of the DFIG-WT behaves like the internal voltage $E_{\rm q}$ of a SG. In other words, if the angle δ of a DFIG-WT has similar dynamics with the $\delta_{\rm SG}$ of a SG in frequency excursion events, then the DFIG-WT will take part in the frequency regulation process as well. This can be realized by adjusting the output of the PLL, i.e., $\theta_{\rm PLL}$. Then the control of δ can be realized by adding $\Delta\delta$ or $-\Delta\delta$ to $\theta_{\rm PLL}$.

3 Bang-bang Phase Angle Controller Design

In order to mimic the frequency response behaviour of a SG, the added phase angle $\Delta\delta$ should satisfy $\Delta\delta > 0$ when $\Delta\omega_{\rm s} < 0$ and $\Delta\delta < 0$ when $\Delta\omega_{\rm s} > 0$ as illustrated in Fig. 1 (b). For this purpose, the following BPAC is designed.

For the simplicity of analysis, assume $R_{\rm eq} = 0$. Then the active power generated by the DFIG-WT is $P_{\rm e} = \frac{E_{\rm ms}V_{\rm s}}{\omega_{\rm s}L_{\rm eq}}\sin(\delta)$. The external power grid can be equivalent with a SG, where the grid frequency is the electrical rotational speed of its rotor. Using this representation, the problem of the frequency regulation is transformed to the problem of regulating the rotor speed of the equivalent SG. The active power from the DFIG-WT actually acts as an input power to the equivalent SG. Consequently, the motion equation of the equivalent SG can be written as follows.

$$\begin{cases} \dot{\delta}_{\rm SG} = \omega_{\rm s}\cdot\omega_{\rm nom} \\ \dot{\omega}_{\rm s} = \frac{1}{M}(P_{\rm mSG} + P_{\rm e} - P_{\rm eSG} - D\Delta\omega_{\rm s}) \end{cases} \tag{2}$$

where $\delta_{\rm SG}$ is the equivalent rotor angle, M denotes the equivalent inertia constant, $P_{\rm mSG}$ is the equivalent mechanical power input of the SG, $P_{\rm eSG}$ is the equivalent active power output of the equivalent SG, D denotes the equivalent damping coefficient, $P_{\rm e}$ is the active power output of the SG, and $\omega_{\rm nom}$ is the nominal rotation speed of the SG.

By defining $x = [x_1 \quad x_2]^\top = [\delta_{\rm SG} \quad \omega_{\rm s}]^\top$ as state variables, $u = \sin(\delta)$ as the control variable, and $y = x_2 = \omega_{\rm s}$ as the output variable of (2), (2) can be written as,

$$\dot{y}(t) = f(x) + g(x)u(t)$$

where $f(x) = (P_{\rm mSG} - P_{\rm eSG} - D\Delta x_2)/M$, $g(x) = \frac{E_{\rm ms}V_{\rm s}}{Mx_2L_{\rm eq}}$, and $u(t) = \sin(\delta)$. As $g(x) > 0$, the relative degree of $y(t)$ with respect to $u(t)$ is $r = 1$. A first-order BPAC is designed for the regulation of $y(t)$.

The BPAC is a logic-based controller [17], which is driven by the error of system frequency. The control variables generated by the BPAC are bang-bang with three control values, i.e. the maximum U^+ of the control variable, the minimum U^- of the control variable and the neutral value U^0 [19]. The switching logic of the first-order BPAC are as follows [19].

$$\begin{aligned} &q(t) = \mathcal{G}(e(t), \varphi_0^+ - \varepsilon_0^+, \varphi_0^- + \varepsilon_0^-, q(t-)) = \\ &\begin{cases} -1, \text{ if } (e(t) \geq \varphi_0^+ - \varepsilon_0^+) \vee (q(t-) = -1 \wedge e(t) > 0) \\ 0, \text{ if } (e(t) = 0) \vee (q(t-) = 0 \wedge \varphi_0^- + \varepsilon_0^- < e(t) < \varphi_0^+ - \varepsilon_0^+) \\ +1. \text{ if } (e(t) \leq \varphi_0^- + \varepsilon_0^-) \vee (q(t-) = +1 \wedge e(t) < 0) \end{cases} \\ &q(0-) \in \{+1, 0, -1\} \end{aligned} \tag{3}$$

where $q(t) \in \{+1, 0, -1\}$, $e(t) = \omega_{\rm s} - \omega_{\rm s\_ref}$ is the system frequency deviation, $q(t-) := \lim_{\varepsilon\to 0+} q(t-\varepsilon)$ [19], $\varphi_0^\pm$ and $\varepsilon_0^\pm$ are funnel parameters. Based on the logic output $q(t)$, BPAC outputs

$$u(t) = \begin{cases} \sin\delta|_{\rm min}, & \text{if} \quad q(t) = -1 \\ 0, & \text{if} \quad q(t) = 0 \\ \sin\delta|_{\rm max}, & \text{if} \quad q(t) = +1 \end{cases} \tag{4}$$

where $\sin\delta|_{\rm min}$ is the minimum of $\sin(\delta)$, and $\sin\delta|_{\rm max}$ is the maximum of $\sin(\delta)$. Under the normal operating conditions of a DFIG-WT, δ is a small value within the interval $(0, \pi/2)$. Hence, $\sin\delta|_{\rm min}$ and $\sin\delta|_{\rm max}$ can be realized by adding $-\Delta\delta$ and $\Delta\delta$ to

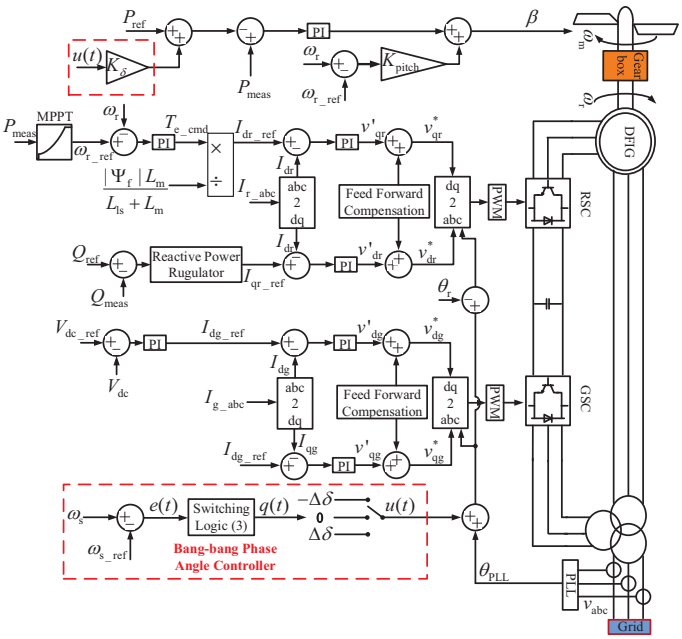

Fig. 2: The control configuration of the DFIG-WT supplemented with a BPAC.

$\theta_{\rm PLL}$, where $\Delta\delta \in (0, \delta_0)$ and δ_0 is the initial value of the angle between $\vec{E}_{\rm ms}$ and $\vec{V}_{\rm s}$. To this end, the control law of the BPAC can be transformed to

$$u(t) = \begin{cases} -\Delta\delta, & \text{if} \quad q(t) = -1 \\ 0, & \text{if} \quad q(t) = 0 \\ \Delta\delta, & \text{if} \quad q(t) = +1. \end{cases} \tag{5}$$

The control configuration of the DFIG-WT supplemented with a BPAC is illustrated in Fig. 2. The structure of the pitch angle controller of the DFIG-WT is also illustrated therein. The pitch angle controller is composed of a rotor speed control loop and an active power control loop. The rotor speed control loop is implemented to prevent the over-speed of the DFIG-WT. The active power control loop is made up of a start-up control loop ($P_{\rm ref}$ loop) and a bang-bang control loop (K_δ loop), the objectives of which are explained as follows.

Since the investigation undertaken in this paper considers the switching behaviour of power electronics converters, the simulation cannot start to operate from the steady state. A start-up control loop is implemented on the pitch angle controller, and the active power of the DFIG-WT is regulated at $P_{\rm set}$ at the beginning of the simulation. Therefore, $P_{\rm ref}$ depicted in Fig. 2 is $P_{\rm ref} = P_{\rm set}$ at the beginning of a simulation and $P_{\rm ref} = P_{\rm meas}$ after the simulated system reaches the steady-state operation point. At the steady-state operation point, system frequency converges to its nominal value and the output of the BPAC is 0 rad. The K_δ loop does not influence the pitch angle in the steady-state. This will lead to that the pitch angle of the DFIG-WT is not zero at steady-state and the DFIG-WT operates at the de-loading mode, which facilitates its frequency support capability as discussed in [20].

Due to the BPAC regulates the active power of the wind turbine in a bang-bang manner, the active power increase of the wind turbine is enabled by the deceleration of the rotor at the beginning of a frequency drop event. Because of the rotor speed control loop of the controller of the RSC as shown in Fig. 2, the rotor of DFIG-WT is controlled to accelerate at the middle of the frequency drop event. The the active power of the wind turbine declines, which will result in a secondary frequency drop. By feeding the output of the BPAC back into the pitch controller, the pitch angle of the DFIG-WT is regulated in a coordinated manner to increase the mechanical power input to the wind turbine at the beginning of the frequency

drop event. In this way, the mechanical power input of the wind turbine is elevated for rotor speed recovery without a secondary active power drop of the wind turbine. The secondary frequency drop of the external grid is prevented in the frequency recovery process. The input $\omega_{\rm s}$ of the BPAC can be the frequency measured at a load bus or the frequency of a SG of the external system, both of which indicates the frequency of the external power grid.

4 Small-signal Stability Analysis of Power Systems With DFIG-WTs Penetration

Referring to (2), the small-signal form of the motion equation of the SG is

$$\begin{cases} \Delta\dot{\delta}_{\rm SG} = \Delta\omega_{\rm s}\omega_{\rm nom} \\ \Delta\dot{\omega}_{\rm s} = \dfrac{1}{M}(\Delta P_{\rm mSG} + \Delta P_{\rm e} - \Delta P_{\rm eSG} - D\Delta\omega_{\rm s}) \end{cases} \tag{6}$$

where it is assumed that the mechanical power input of the SG is constant, i.e. $\Delta P_{\rm mSG} = 0$, and $\Delta P_{\rm eSG} = \frac{\partial P_{\rm eSG}}{\partial \delta_{\rm SG}}\Delta\delta_{\rm SG}$ with $\frac{\partial P_{\rm eSG}}{\partial \delta_{\rm SG}} > 0$ [21]. Besides, $\Delta P_{\rm e}$ can be obtained as follows.

Referring to Fig. 1 (b), the expression of $\overrightarrow{E}_{\rm ms}$ can be rewritten as $\overrightarrow{E}_{\rm ms} = E_{\rm ms}(\cos\delta + j\sin\delta)$ on the assumption that $\overrightarrow{V}_{\rm s} = V_{\rm s}\angle 0^\circ$. It follows that $\overrightarrow{I}_{\rm eq} = \frac{E_{\rm ms}\cos\delta + jE_{\rm ms}\sin\delta - V_{\rm s}}{R_{\rm eq}+j\omega_{\rm s}L_{\rm eq}}$, the active power generated by the DFIG-WT is $P_{\rm e} = {\rm Re}(\overrightarrow{V}_{\rm s}\overrightarrow{I}^{*}_{\rm eq}) = V_{\rm s}I_{\rm eqd}$, where $I_{\rm eqd}$ is the d-axis component of $\overrightarrow{I}_{\rm eq}$. Combining the expressions of $R_{\rm eq}$ and $L_{\rm eq}$, it has $I_{\rm eqd} = \frac{R_{\rm eq}(E_{\rm ms}\cos\delta - V_{\rm s}) + E_{\rm ms}\omega_{\rm s}L_{\rm eq}\sin\delta}{R_{\rm eq}^2 + (\omega_{\rm s}L_{\rm eq})^2}$. Hence, it can be shown that

$$\frac{\partial P_{\rm e}}{\partial \omega_{\rm s}} = \frac{V_{\rm s}(E_{\rm ms}\cos\delta - V_{\rm s})\frac{\partial R_{\rm eq}}{\partial \omega_{\rm s}} + E_{\rm ms}V_{\rm s}L_{\rm eq}\sin\delta + E_{\rm ms}V_{\rm s}\omega_{\rm s}\sin\delta\frac{\partial L_{\rm eq}}{\partial \omega_{\rm s}}}{R_{\rm eq}^2 + (\omega_{\rm s}L_{\rm eq})^2} + \frac{(2R_{\rm eq}\frac{\partial R_{\rm eq}}{\partial \omega_{\rm s}} + 2\omega_{\rm s}^2 L_{\rm eq}\frac{\partial L_{\rm eq}}{\partial \omega_{\rm s}})[R_{\rm eq}V_{\rm s}(E_{\rm ms}\cos\delta - V_{\rm s}) + E_{\rm ms}V_{\rm s}\omega_{\rm s}L_{\rm eq}\sin\delta]}{[R_{\rm eq}^2 + (\omega_{\rm s}L_{\rm eq})^2]^2} \tag{7}$$

where

$$\frac{\partial R_{\rm eq}}{\partial \omega_{\rm s}} = \frac{(2\omega_{\rm s} - \omega_{\rm r})L_{\rm m}^2 R_{\rm r}[R_{\rm r}^2 + (\omega_{\rm s} - \omega_{\rm r})^2 L_{\rm r}^2] - 2(\omega_{\rm s} - \omega_{\rm r})^2 L_{\rm r}^2 \omega_{\rm s} L_{\rm m}^2 R_{\rm r}}{[R_{\rm r}^2 + (\omega_{\rm s} - \omega_{\rm r})^2 L_{\rm r}^2]^2}$$

and

$$\frac{\partial L_{\rm eq}}{\partial \omega_{\rm s}} = -\frac{2L_{\rm m}^2 L_{\rm r}(\omega_{\rm s} - \omega_{\rm r})R_{\rm r}^2}{[R_{\rm r}^2 + (\omega_{\rm s} - \omega_{\rm r})^2 R_{\rm r}^2]^2}.$$

Moreover, it can be demonstrated that

$$\frac{\partial P_{\rm e}}{\partial \delta} = \frac{-R_{\rm eq}V_{\rm s}E_{\rm ms}\sin\delta + E_{\rm ms}V_{\rm s}\omega_{\rm s}L_{\rm eq}\cos\delta}{R_{\rm eq}^2 + (\omega_{\rm s}L_{\rm eq})^2} \tag{8}$$

Therefore, it has $\Delta P_{\rm e} = \frac{\partial P_{\rm e}}{\partial \omega_{\rm s}}\Delta\omega_{\rm s} + \frac{\partial P_{\rm e}}{\partial \delta}\Delta\delta$.

According to (6), the poles of the small-signal model of the SG with no DFIG-WTs penetration are $s_{1,2} = \frac{-D \pm \sqrt{D^2 - 4M\frac{\partial P_{\rm eSG}}{\partial \delta_{\rm SG}}\omega_{\rm nom}}}{2M}$. The damping coefficient of the SG is usually rendered positive by installing power system stabilizers.

In the case where DFIG-WTs are connected with SGs, the small-signal model of a SG-based power system with DFIG-WT penetration can be illustrated as shown in Fig. 3 (a). In this case, the poles of the closed-loop system are $s_{1,2} = \frac{-(D - \frac{\partial P_{\rm e}}{\partial \omega_{\rm s}}) \pm \sqrt{(D - \frac{\partial P_{\rm e}}{\partial \omega_{\rm s}})^2 - 4M\frac{\partial P_{\rm eSG}}{\partial \delta_{\rm SG}}\omega_{\rm nom}}}{2M}$. Hence, the impact of the DFIG-WT with respect to the frequency stability of power systems is determined by the sign of $\frac{\partial P_{\rm e}}{\partial \omega_{\rm s}}$. Use the DFIG-WT, whose parameters are presented in Table 1, as an example. Let the grid frequency $\omega_{\rm s}$ be within [0.96, 1.04] p.u. and the angle δ between $\overrightarrow{E}_{\rm ms}$ and $\overrightarrow{V}_{\rm s}$ be within [0, π/6], then $\frac{\partial P_{\rm e}}{\partial \omega_{\rm s}}$ versus $\omega_{\rm s}$ and δ can be presented as shown in Fig. 3 (b), where the internal voltage of the DFIG-WT satisfies $\overrightarrow{E}_{\rm ms} = 0.9968\angle 17.733^\circ$, the terminal bus voltage satisfies $\overrightarrow{V}_{\rm s} = 1\angle 0^\circ$, and $\omega_{\rm r}$ =1.2 p.u. From Fig. 3 (b), it can be observed that $\frac{\partial P_{\rm e}}{\partial \omega_{\rm s}} > 0$ holds on the investigated domain of $\omega_{\rm s}$ and δ. Hence,

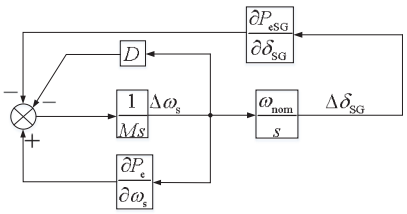

(a) The small-signal model of the SG with DFIG-WTs penetration.

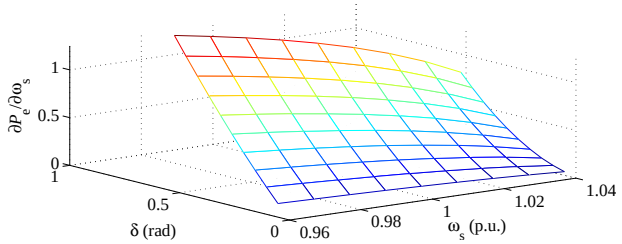

(b) $\frac{\partial P_{\rm e}}{\partial \omega_{\rm s}}$ versus $\omega_{\rm s}$ and δ.

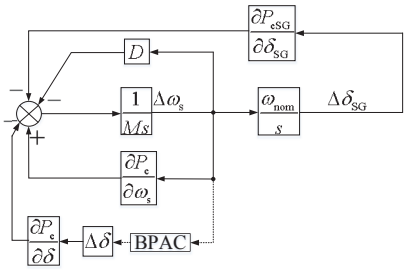

(c) The linearized model of the SG with the DFIG-WT controlled by the BPAC.

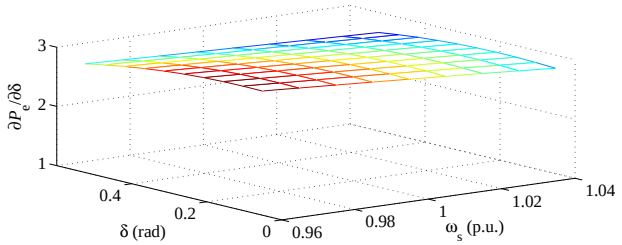

(d) $\frac{\partial P_{\rm e}}{\partial \delta}$ versus $\omega_{\rm s}$ and δ.

Fig. 3: The small-signal model of the SG with a DFIG-WT penetration and $\frac{\partial P_{\rm e}}{\partial \omega_{\rm s}}$ versus $\omega_{\rm s}$ and δ, and the linearized model of the SG with a DFIG-WT controlled by the BPAC and $\frac{\partial P_{\rm e}}{\partial \delta}$ versus $\omega_{\rm s}$ and δ.

the penetration of DFIG-WT drives the closed-loop poles of the SG towards right, and thus deteriorates the frequency stability of the SG.

According to (3) and (5), the control law of the BPAC can be simplified as $u(t) \approx -\Delta\delta{\rm sign}(\Delta\omega_{\rm s})$ when $u(t) \neq 0$, $|\varphi_0^- + \varepsilon_0^-| \approx 0$, and $|\varphi_0^+ - \varepsilon_0^+| \approx 0$ hold. Therefore, linearized model of SG with the DFIG-WT controlled by the BPAC can be illustrated as shown in Fig. 3 (c). The poles of the closed-loop system are $s_{1,2} = \frac{-(D - \frac{\partial P_{\rm e}}{\partial \omega_{\rm s}} + \frac{\partial P_{\rm e}}{\partial \delta}\delta'(t)) \pm \sqrt{(D - \frac{\partial P_{\rm e}}{\partial \omega_{\rm s}} + \frac{\partial P_{\rm e}}{\partial \delta}\delta'(t))^2 - 4M\frac{\partial P_{\rm e}}{\partial \delta_{\rm SG}}\omega_{\rm nom}}}{2M}$, where $\delta'(t) = \Delta\delta/|\Delta\omega_{\rm s}(t)|$. The influence of the DFIG-WT reflects from the sign of the term $-\frac{\partial P_{\rm e}}{\partial \omega_{\rm s}} + \frac{\partial P_{\rm e}}{\partial \delta}\delta'(t)$. For the DFIG-WT specified in Table 1, $\frac{\partial P_{\rm e}}{\partial \delta}$ versus $\omega_{\rm s}$ and δ is illustrated in Fig. 3 (d). From Fig. 3 (d), it can be seen that $\frac{\partial P_{\rm e}}{\partial \delta} > 0$ holds on the investigated domain of $\omega_{\rm s}$ and δ. Regarding $\Delta\delta > 0$, the implementation of the BPAC is able to drive the closed-loop poles of the system towards left. Especially, under a nominal operating condition, i.e., $\omega_{\rm s} = 1$, $\delta = 0.3059$ rad, and $P_{\rm e}$=0.9 p.u., it has $\frac{\partial P_{\rm e}}{\partial \delta} = 2.92$. Let $\Delta\delta = 0.3$ rad and $|\Delta\omega_{\rm s}| = 0.0333$ p.u., then the compensation of

the BPAC loop is $\frac{\partial P_e}{\partial \omega_s}\delta' = 26.31$. Under the same operating condition with $\Delta\omega_s = 0.0333$ p.u., $-\frac{\partial P_e}{\partial \omega_s} = -0.691$ holds and it has $-\frac{\partial P_e}{\partial \omega_s} + \frac{\partial P_e}{\partial \delta}\delta'(t) > 0$. Therefore, the side-effect introduced by the $\frac{\partial P_e}{\partial \omega_s}$ loop can be completely eliminated by the BPAC loop, and the BPAC further improves the damping ability of the DFIG-WT with respect to the oscillations of ω_s.

According to the above analysis, a higher value of $\Delta\delta$ will result in more active power support from the DFIG-WT. Nevertheless, the selection of $\Delta\delta$ should also consider the internal stability of the DFIG-WT system. For the DFIG-WT with the parameters presented in Table 1, the closed-loop poles of the DFIG-WT system with $\Delta\delta$ in the range of [0.1 0.5] rad are as illustrated in Fig. 4. As can be seen, a pair of poles move to the right-half complex plain as $\Delta\delta$ increases to 0.5 rad. Therefore, $\Delta\delta$ is selected as 0.3 rad here for the internal stability of the DFIG-WT system.

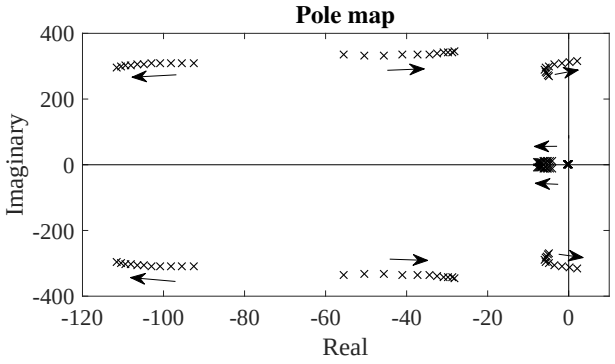

Fig. 4: Pole maps of the DFIG-WT with $\Delta\delta$ increasing from 0.1 rad to 0.5 rad.

5 Simulation Results

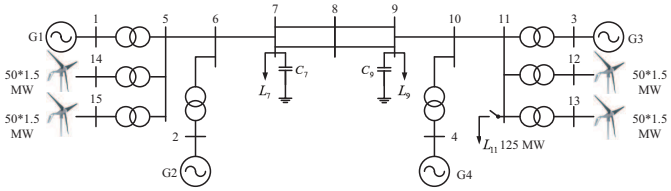

Fig. 5: The schematic of the wind power penetrated multi-machine power system.

Table 1 The parameters of the DFIG-WT

Para.	Value	Para.	Value	Para.	Value
P_n	1.5 MW	f_n	60 Hz	K_δ	0.4
R_s	0.023 p.u.	L_{ls}	0.18 p.u.	R_r	0.016 p.u.
L_{lr}	0.16 p.u.	L_m	2.9 p.u.	H_i	0.685 s
p	3	R_g	0.003 p.u.	L_g	0.3 p.u.
V_{dc}	1150 V	C	1×10^{-2} F	H_t	4.32 s
V_{wind}	15 m/s	φ_0^+	0.4	φ_0^-	-0.4
ε_0^+	0.35	ε_0^-	0.35	u(0)	0 rad

Simulation studies were undertaken on a wind power penetrated multi-machine power system shown in Fig. 5, which was constructed based on the four-generator eleven-bus power system of [21]. In the simulation models, the switching process of power electronics converters are considered and wind farms are simulated with an integrated model of the DFIG-WT. Simulation results were obtained with a discrete power system model in Matlab/Simulink and the simulation step length was 5μs. In order to reduce the time consumption, all the simulation models are operated from the initial states obtained from the steady-state variables stored by the previous simulations. The parameters of the DFIG-WT are presented in Table 1, where P_n is the rated power of the DFIG-WT, H_i denotes the inertia constant of the induction generator, H_t represents the inertia constant of the wind turbine, p is the number of pole pairs of the rotor, R_g and L_g represent the filter resistance and inductance of the grid-side converter, V_{dc_nom} denotes the nominal voltage of the dc-link capacitor of the DFIG-WT, C is the capacity of the dc-link capacitor [18].

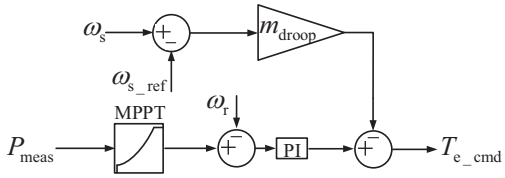

Fig. 6: The schematic of DRC.

Two 75 MW DFIG-WT-based wind farms are collected on bus 5 and bus 11, respectively. A 125 MW load is added on bus 11. The active power output of G_1 was set to 565 MW. The other parameters of the test system are the same as those presented in [21]. The primary frequency support performance of the DFIG-WT with BPAC is compared with those with original configuration and a droop controller (DRC). The original configuration of the DFIG-WT can be illustrated with Fig. 2 without the parts framed by the dashed lines. The DRC is realized by a frequency droop controller implemented on the torque control loop of the rotor-side controller, the schematic of which is shown by Fig. 6. The droop coefficient m_{droop} is set as 4 such that 25% system frequency drop will result in 100% torque increase of the DFIG-WT. This is chosen based on a tradeoff between the steady-state performance and the active power support effort of the DFIG-WT.

5.1 Case A: Grid Frequency is Higher Than the Rated Value

The primary frequency response of the DFIG-WT controlled by the BPAC is investigated in the case where load L_{11} trips at $t = 0.5$s. The inputs to BPACs are the frequency error on node 7.

Primary frequency support performance of wind farm 12 (WF_{12}) is analyzed here, and we observed that the other wind farms have similar dynamics. Once the load frequency deviation of bus 7 increases over 0.05 Hz due to the load trip, the BPAC generates a negative control value as depicted in Fig. 7 (c), and the pitch angle β increases in Fig. 7 (d). It follows that the active power output of the DFIG-WT controlled by the BPAC is reduced, which is illustrated in Fig. 7 (a), such that the accelerating power of the test system is decreased. As depicted in Fig. 8 (a)-(c), the rotor speed of the SGs presents smaller deviations in the system with the BPAC than in the systems with the original configuration and the DRC, respectively. Moreover, less error of system frequency can be found in the power system with the BPAC installed in contrast to the system with the original configuration and the DRC respectively as shown in Fig. 8 (d).

It is noticed that the pitch angle β of the DFIG-WT is not started at zero. This is due to that the DFIG-WT is operated at the de-loading mode at the beginning to enable its primary frequency regulation capability. This technique was reviewed in [20] and referred to as the pitching de-loading technique of wind turbines, which enables wind turbines to participate in the primary and secondary frequency regulation. Moreover, the pitch angle under the control of DRC presents a decrease at the beginning of the post-disturbance process as presented in Fig. 7 (d). This is caused by the active power control loop

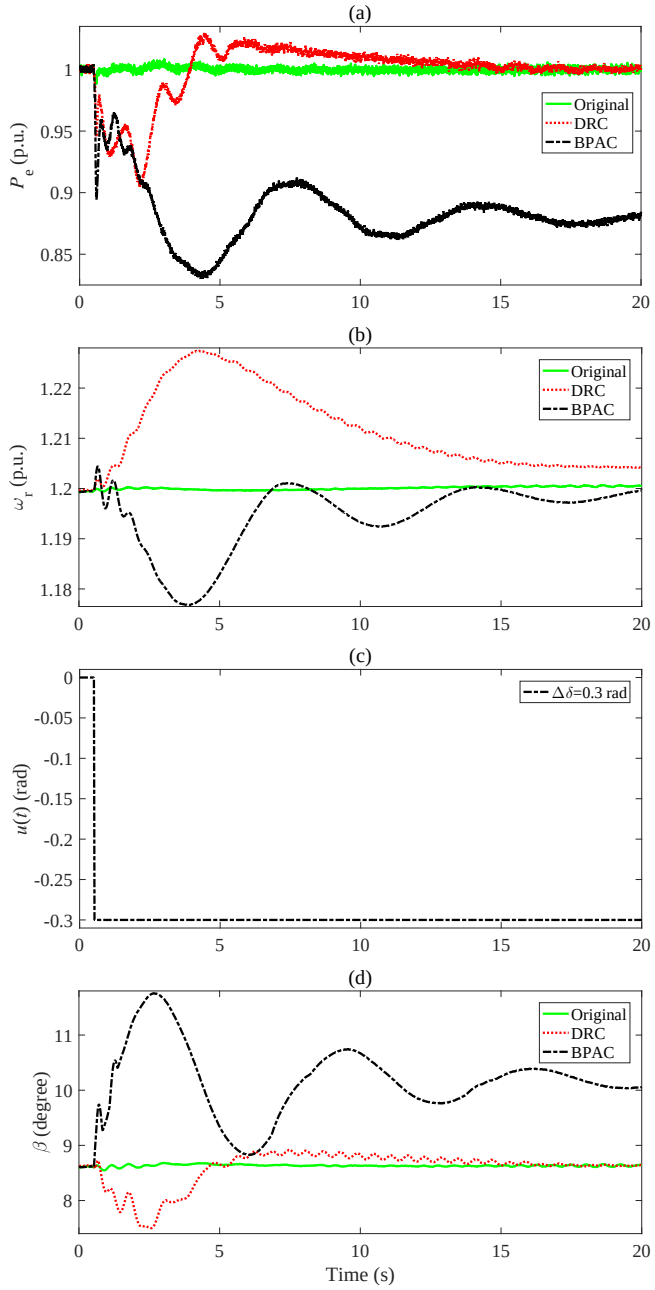

Fig. 7: Primary frequency control performance of WF_{12} observed in the scenario where grid frequency is higher than the rated value ((a) Active power generated by the DFIG-WT (b) Rotor speed (c) Control signal from BPAC (d) Pitch angle β).

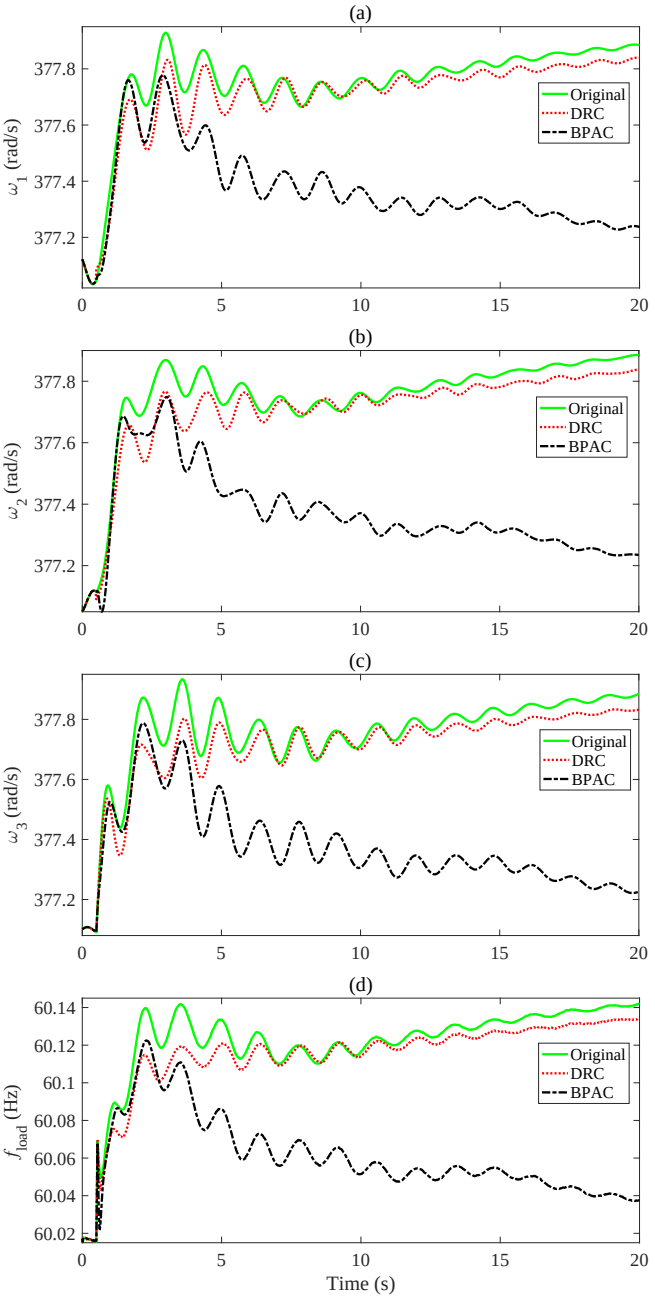

Fig. 8: Rotor speed of SGs and load frequency observed in the scenario where a load trip occurs in the test system ((a) The rotor speed of G_1 (b) The rotor speed of G_2 (c) The rotor speed of G_3 (d) The system frequency measured at the load bus 7).

of the pitch angle controller shown in Fig. 2. At the beginning of the post-disturbance process, the control effort of the active power control loop overrides that of the rotor speed control loop in the pitch angle controller, thus the pitch angle of the DFIG-WT decreases due to the drop of its active power output.

With respect to the dynamics within the DFIG-WT, the DFIG-WT with the DRC offers frequency support to the external grid as well, which is illustrated by Fig. 7 (a). The reduced active power output of the DFIG-WT is transformed as the kinetic energy of its rotor as justified in Fig. 7 (b). However, due to the effort of the active power control loop in the pitch angle controller, the pitch angle of the wind power generator with the DRC is decreased to maintain the active power output of the DFIG-WT at the pre-fault value as presented in Fig. 7 (d). Consequently, the DFIG-WT with the DRC cannot provide continuous frequency regulation, and this results in more system frequency deviation as illustrated in Fig. 8 (d). Moreover, the DFIG-WT with the DRC implemented shows over-speed in its rotor as depicted in Fig. 7 (b), which is undesirable for the reliable operation of the DFIG-WT.

5.2 Case B: Grid Frequency is Lower Than the Rated Value

The primary frequency control performance of the BPAC is evaluated in comparison with the DRC in the case where grid frequency is below the rated value. Load 11, which is not connected to the grid at $t = 0$s, is switched on operation at $t = 0.5$s. The inputs to the BPACs of the DFIG-WTs of WF_{12} and WF_{13} are the rotor speed deviation of G_4. The inputs to the BPACs of the DFIG-WTs of WF_{14} and WF_{15} are the rotor speed deviation of G_1. The four power plants have an initial active power outputs of 0.8 p.u., respectively, such

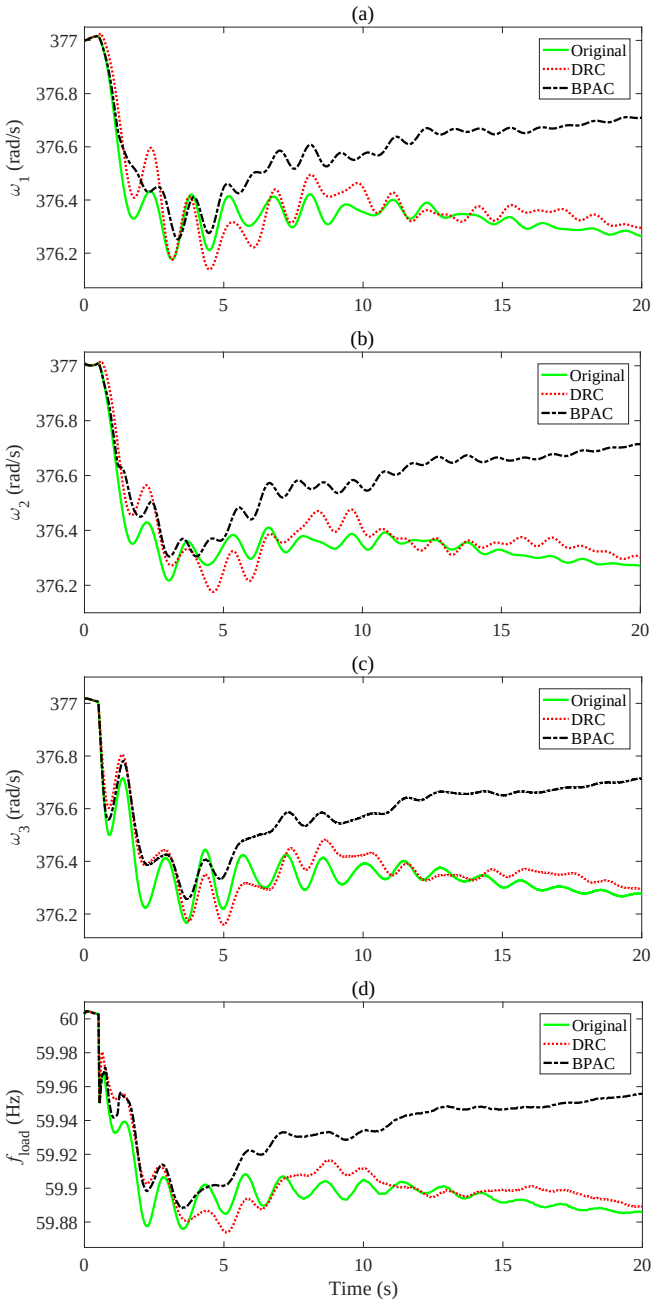

Fig. 9: Rotor speed of SGs and load frequency observed in the scenario where load 11 is connected to the test system ((a) The rotor speed of G_1 (b) The rotor speed of G_2 (c) The rotor speed of G_3 (d) Grid frequency measured at the load bus 7).

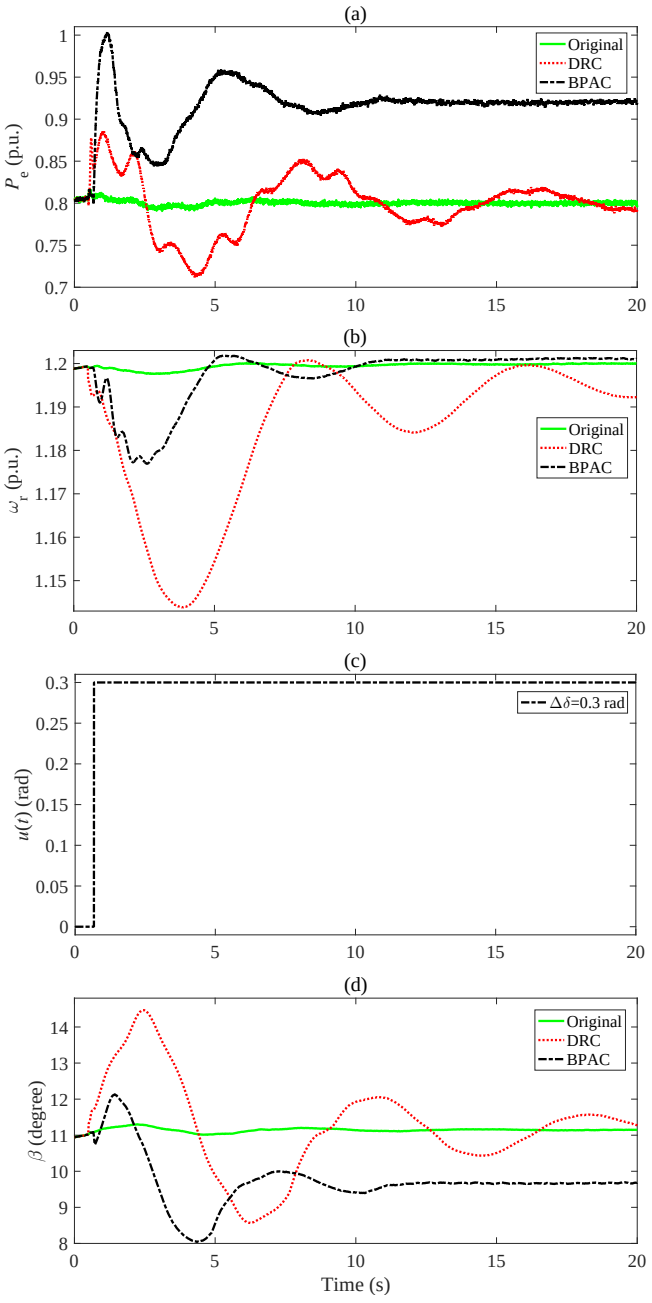

Fig. 10: Primary frequency control performance of WF_{12} observed in the scenario where grid frequency is lower than the rated value ((a) Active power (b) Rotor speed (c) Control signal from BPAC (d) Pitch angle).

that they have 0.2 p.u. active power margin for primary frequency support.

The frequency dynamics of the SG-side of the power system is depicted in Fig. 9. As can be observed, the rotor speed of G_1, G_2, and G_3 of the power system having the BPAC installed presents less oscillations than those of the systems with the original configuration and the DRC, respectively, as shown in Fig. 9(a)-(c). The system frequency measured on node 7 is illustrated in Fig. 9 (d). Comparing the results presented in Fig. 8 and Fig. 9, we can find that more oscillations are found in the case of load trip. This can be reveal by the modal analysis of the test system at the operation point of case A and case B, respectively. Table 2 illustrates the oscillatory modes of the test system in case A and case B, where f denotes the oscillation frequency of the mode and ξ represents the damping ratio of the mode. From Table 2, it can be observed that system oscillatory modes of case B have higher damping ratio and lower oscillation frequency than those of case A, which meets the phenomenon presented by Fig. 8 and Fig. 9.

As load 11 is switched on, the system frequency drops and the BPAC generates a $\Delta\delta$ of 0.3 rad presented in Fig. 10(c). The reference P_{ref} of active power output is also increased in the pitch angle controller. Referring to Fig. 10 (a), the active power output of the DFIG-WT increases as a result of the combined effort of the deceleration of rotor, shown in Fig. 10 (b), and the reduced pitch angle, presented in Fig. 10 (d). When the effort of the rotor speed deviation loop overrides that of the active power control loop in the pitch angle controller presented in Fig. 2, β starts to decrease and finally stabilizes to a novel equilibrium as shown in Fig. 10 (d).

In contrast, the DFIG-WT with the DRC offers primary frequency support completely by the deceleration of rotor as shown in Fig. 10 (b). This can improve the active power output of the DFIG-WT as

Table 2 Oscillatory Modes of the Test System

Case	Inter-area mode	Local mode 1	Local mode 2
Case B	- $0.1734 \pm j3.9669$ ($f = 0.6313$, $\xi = 0.0437$)	- $1.2400 \pm j5.4383$ ($f = 0.8655$, $\xi = 0.2223$)	- $0.6821 \pm j5.8477$ ($f = 0.9307$, $\xi = 0.1159$)
Case A	- $0.1543 \pm j4.0629$ ($f = 0.6466$, $\xi = 0.0379$)	- $1.2521 \pm j5.5282$ ($f = 0.8798$, $\xi = 0.2209$)	- $0.5832 \pm j5.8841$ ($f = 0.9365$, $\xi = 0.0986$)

well as presented in Fig. 10 (a). However, the recovery of the rotor speed of the DFIG-WT leads to the secondary active power drop as illustrated in Fig. 10 (a). Due to the positive overshot of the pitch angle of turbine blades at the beginning of the primary frequency response process shown in Fig. 10 (d), the system with DRC shows more frequency deviation and lower frequency nadir than that with the BPAC as manifested in Fig. 9 (d).

6 Discussions

The BPAC is proposed here for fast frequency response of DFIG-WTs. The conventional continuous controllers, like droop controllers, suffer from the trade-off between the response speed and overshoot. As a supplementary control effort for fast frequency response, the constant $\Delta\delta$ is preferred in the logic driven bang-bang control processes. If severe frequency deviation events are considered, the BPAC can be implemented combined with the conventional droop controllers. Then the BPAC can provided fast frequency response in the beginning of a severe frequency deviation event, and then the droop controller can offer slow but sustained frequency support. This is the prime motivation for the design of the BPAC with constant $\Delta\delta$ in this paper.

7 Conclusions

This paper has introduced a BPAC for the primary frequency control of DFIG-WTs. By comparing the dynamics of the internal voltage of a SG and that of a DFIG-WT, it obtains that the internal voltage vector of a DFIG-WT is relatively static with respect to its terminal bus voltage vector, which results in the DFIG-WT having poor inertial support capability. The BPAC was designed mainly based on this conclusion. The small-signal analysis of the closed-loop system, consisting of a DFIG-WT and a SG, manifests that the implementation of the BPAC is able to improve the frequency stability of the power system. Considering that all topologies of the inter-connection of DFIG-WT-based wind farms and SG-based power grids can be transformed to the closed-loop system studied in this paper, the small-signal analysis presented here is simple but effective.

Results obtained by simulations are consistent with the conclusions of small-signal analysis. The DFIG-WTs controlled by the BPAC outperform the ones with the original configuration and the DRC, respectively. Less oscillations are observed in the rotor speed of SGs and lower load frequency excursions are found in the power systems with the BPAC installed than those without the BPAC. The DFIG-WT with the BPAC provides primary frequency control performance through the combined effort of rotor kinetic energy regulation and the pitch angle control. Compared with the DRC, the BPAC does not have the problem of rotor speed recovery. Therefore, secondary frequency drop is eliminated in the power system with the BPAC. Moreover, the DFIG-WT with the DRC faces the potential danger of the over-speed of the rotor. Therefore, elaborate monitoring and configuration of the operating condition of DFIG-WTs are needed before the DRC is applied.

The BPAC is simple in structure and it only involves logic calculation. The BPAC can be easily applied in other inverter-based voltage sources for primary frequency support.

8 Acknowledgements

This work was supported in part by the State Key Program of National Science of China under Grant 51437006, the Guangdong Innovative Research Team Program under Grant 201001N0104744201, and China Scholarship Council (CSC).

9 References

[1] Liu, Y., Wu, Q. H., Zhou, X. X.:'Co-ordinated multiloop switching control of DFIG for resilience enhancement of wind power penetrated power systems', IEEE Trans. Sustain. Energy, 2016, 7, (3), pp. 1089–1099

[2] Zhang, W., Fang, K.: 'Controlling active power of wind farms to participate in load frequency control of power systems', IET Gener. Transm. Dis., 2017, 11, (9), pp. 2194–2203

[3] Leon, A. E., Revel, G., Alonso, D. M., etal.: 'Wind power converters improving the power system stability', IET Gener. Transm. Dis., 2016, 10, (7), pp. 1622–1633

[4] Lalor, G., Mullane, A., O'Malley, M.: 'Frequency control and wind turbine technologies', IEEE Trans. Power Syst., 2005, 20, (4), pp. 1905–1913

[5] Xia, J., Dyśko, A., O'Reilly, J.: 'Future stability challenges for the UK network with high wind penetration levels', IET Gener. Transm. Dis., 2015, 9, (11). pp. 1160–1167

[6] Attya, A. B., Hartkopf, T.: 'Wind turbine contribution in frequency drop mitigation-modified operation and estimation released supportive energy', IET Gener. Transm. Dis., 2014, 8, (5), pp. 862–872

[7] Driesen, J., Visscher, K.: 'Virtual synchronous generators'. Proc. Power and Energy Society General Meeting-Conversion and Delivery of Electrical Energy in the 21st Century, July 2008, pp. 1–3

[8] Arani, M. F., EI-Saadany, E. F.:'Implementing virtual inertia in DFIG-based wind power generation', IEEE Trans. Power Syst., 2013, 28, (2), pp. 1373–1384

[9] Choi, J. W., Heo, S. Y., Kim, M. K.: 'Hybrid operation strategy of wind energy storage system for power grid frequency regulation', IET Gener. Transm. Dis., 2016, 10, (3), pp. 736–749

[10] Ekanayake, J., Jenkins, N.: 'Comparison of the response of doubly fed and fixed-speed induction generator wind turbines to changes in network frequency', IEEE Trans. Energy Convers., 2004, 19, (4), pp. 800–802

[11] Solanki, A., Nasiri, A., Bhavaraju, V., etal.: 'A new framework for micro-grid management: Virtual droop control', IEEE Trans. Smart Grid, 2016, 7, (2), pp. 554–566

[12] Zhong, Q. C., Nguyen, P. L., Ma, Z., etal.: 'Self-synchronized synchronverters: Inverters without a dedicated synchronization unit', IEEE Trans. Power Electron., 2014, 29, (2), pp. 617–630

[13] Zhong, Q., Weiss, G.: 'Synchronverters: Inverters that mimic synchronous generators', IEEE Trans. Ind. Electron., 2011, 58, (4), pp. 1259–1267

[14] Wang, S., Hu, J., Yuan, X., etal.: 'On inertial dynamics of virtual-synchronous-controlled DFIG-based wing turbines', IEEE Trans. Energy Convers., 2015, 30, (4), pp. 1691–1702

[15] Kang, M., Kim, K., Muljadi, E., etal.: 'Frequency control support of a doubly-fed induction generator based on the torque limit', IEEE Trans. Power Syst., 2016, 31, (6), pp. 1–9

[16] He, W., Yuan, X., Hu, J.: 'Inertia provision and estimation of PLL-based DFIG wind turbines', IEEE Trans. Power Syst., 2016, 32, (1), pp. 1–10

[17] Liberzon, D., Trenn, S.: 'The bang-bang funnel controller for uncertain nonlinear systems with arbitrary relative degree', IEEE Trans. Autom. Control, 2013, 58, (12), pp. 3126–3141

[18] Liu, Y., Wu, Q. H., Zhou, X. X.: 'Coordinated switching controllers for transient stability of multi-machine power systems', IEEE Trans. Power Syst., 2016, 31, (5), pp. 3937–3949

[19] Hackl, C., Trenn, S.: 'The bang-bang funnel controller: An experimental verification', PAMM, 2012, 12, (1), pp. 735–736

[20] Daz-Gonzlez, F., Hau, M., Sumper, A., etal.: 'Participation of wind power plants in system frequency control: Review of grid code requirements and control methods', Renewable and Sustainable Energy Reviews, 2014, 34, pp. 551–564

[21] Kundur, P., Balu, N. J., Lauby, M. G.: 'Power System stability and control', McGraw-hill New York, 1994, vol. 7